Trans. Phenom. Nano Micro Scales, 4(2): 28-40, Winter and Spring 2016
7508/tpnms.2016.02.004

ORIGINAL RESEARCH PAPER

MHD Boundary Layer Flow and Heat Transfer of Newtonian Nanofluids over a Stretching Sheet with Variable Velocity and Temperature Distribution

***P.Elyasi*[*,1], *A. R. Shateri*[2]**

Mechanical Engineering Department,Faculty of Mechanical Engineering, Shahrekord University, Shahrekord, I. R.Iran

Received 30 April 2015: revised 1 January 2016: accepted 21 January 2016: available online 28 June 2016

ABSTRACT: Laminar boundary layer flow and heat transfer of Newtonian nanofluid over a stretching sheet with the sheet velocity distribution of the form ($U_W=cX^{\beta}$) and the wall temperature distribution of the form ($T_W=T_\infty+aX^r$) for the steady magnetohydrodynamic (MHD) is studied numerically. The governing momentum and energy equations are transformed to the local non-similarity equations using the appropriate transformations. The set of ODEs are solved using Keller–Box implicit finite-difference method. The effects of several parameters, such as magnetic parameter, volume fraction of different nanoparticles (Ag, Cu, CuO, Al_2O_3 and TiO_2), velocity parameter, Prandtl number and temperature parameter on the velocity and temperature distributions, local Nusselt number and skin friction coefficient are examined. The analysis reveals that the temperature profile increases with increasing magnetic parameter and volume fraction of nanofluid. Furthermore, it is found that the thermal boundary layer increases and momentum boundary layer decreases with the use of water based nanofluids as compared to pure water. At constant volume fraction of nanoparticles, it is also illustrated that the role of magnetic parameter on dimensionless temperature becomes more effective in lower value.

KEYWORDS: *Boundary Layer Flow; MHD; Nanofluid; Stretching Sheet*

Introduction

In the past decade, The analysis of laminar magnetohydrodynamic (MHD) flow and heat transfer have attracted considerable attention in many fields of science and technology because of its wide applications, such as cooling of nuclear reactors during emergency shutdown conditions, metal and polymer extrusion, drawing of plastic sheets, exchangers and chemical processing equipment, the boundary layer control in the field of aerodynamics and many others. Specially to control the behavior of the boundary layer several artificial methods have been developed and out of that, the application of MHD principle is an important method for affecting the flow field in the desired direction by altering the structure of the boundary layer. In recent years, nanofluids have attracted much interest because of their reported superior thermal performance and many potential applications. When nanofluid is added to this subject, it would be of great interest to researchers. Compared to micron-sized particles, nanoparticles are engineered to have larger relative surface area, less particle momentum, high mobility and better suspension stability and importantly increase the thermal conductivity of the mixture. This makes the nanofluids a promising working mediums coolants, lubricants, hydraulic fluids and metal cutting fluids. Further, a negligible pressure drop and mechanical abrasion makes researchers subscribe to nanofluids for the development of the next generation miniaturized heat exchangers. The word "nanofluid" coined by Choi [1] describes a liquid suspension containing ultra-fine particles (diameter less than 50 nm). The ultra-fine particles are usually made by a high-energy-pulsed process from a conductive material. Choi et al [2] showed that the addition of a small amount (less than 1% by volume) of nanoparticles to conventional heat transfer liquids increased the thermal conductivity of the fluid up to approximately two times. Heris et al [3] measured the effect of the addition of 20 nm aluminum oxide particles to water in a constant wall temperature laminar tube flow. They measured an increase of 10–30% in the convective heat transfer coefficient for a Péclet number ranging from 2500–6000 at 2% by volume concentration of Al_2O_3. Hojjat et al [4] investigated experimentally laminar convection heat transfer behavior of three different types of nanofluids flowing through a uniformly heated horizontal circular tube. Nanofluids were made by dispersion of Al_2O_3, CuO, and TiO_2 nanoparticles in an aqueous solution of carboxymethyl cellulose (CMC). All nanofluids as well as the base fluid exhibited shear-thinning behavior. Results of heat transfer experiments indicated that both average and the local heat transfer coefficients of nanofluids were larger than that of the base fluid. The enhancement of heat transfer coefficient increased by increasing nanoparticle loading. Also, they concluded that the thermal entry length of nanofluids was

*Corresponding Author Email: *paymanelyasi@gmail.com*
Tel.: +983814424401; Note. This manuscript was submitted on April 30, 2015; approved on January 1, 2016; published online June 28, 2016.

Nomenclature

		Φ	Volume fraction (%)
B_0	Uniform magnetic field	μ	Effective dynamic viscosity (Pa. s)
T	Temperature	ρ	Density (kg m^{-3})
u	Velocity components along the X axes	η	similarity variable
v	Velocity components along the Y axes	σ	electric conductivity
Nu_x	Local Nusselt number	θ	dimensionless temperature
Re_x	Local Reynolds number ($Re= U_m x/\nu_f$)	β	Sheet velocity exponent
Pr_f	Prandtl number ($Pr_f=\nu_f/\alpha_f$)	ν	kinematic viscosity (m^2s^{-1})
r	Temperature exponent	τ	Shear stress
k	thermal conductivity (W/m.K)	ψ(x,y)	streamline function
f'(η))	Dimensionless velocity		**Subscripts**
Cf_x	Skin friction coefficient	f	Base fluid
Mn	Magnetic parameter	w	Condition on the sheet
		p	Particle
	Greek Symbols	∞	Condition far away from the plate
α	Thermal diffusivity (m^2/s)	nf	Nanofluid

greater than the base fluid and became longer as nanoparticle concentration increased. Several ideas have been proposed to explain the enhanced heat transfer characteristics of nanofluids. For example, Pak and Cho [5] attributed the increased heat transfer coefficients observed in nanofluids to the dispersion of suspended particles.

Xuan and Li [6] suggested that the heat transfer enhancement was the result of increase in turbulence induced by the nanoparticle motion.

Based on his experimental data on water and glycerin based nanofluids, Ahuja [7] concluded that the heat transfer enhancement was caused by the rotation of nanoparticles. However, after an extensive evaluation of the literature, Boungiorno [8] has shown that the high heat transfer coefficients in nanofluids cannot be explained satisfactorily by thermal dispersion [5] or increase in turbulence intensity [6]. He proposed that the analytical model for convective transport in nanofluids must take into account the Brownian diffusion and thermophoresis and the increase in heat transfer coefficient was due to significant decrease in the viscosity of the fluid caused by the large temperature variations in the boundary layers. Fadzilah et al [9] studied the steady magneto-hydrodynamic boundary-layer flow and heat transfer of a viscous and electrically conducting fluid over a stretching sheet with an induced magnetic field. The results of their study show that the velocity and induced magnetic field increase with an increase in the applied magnetic field. Ishak et al [10] studied the steady MHD boundary-layer flow and heat transfer due to a stretching sheet. The result shows that the velocity gradient at the surface increases but the temperature gradient decreases as magnetic parameter increases. Besides, it is shown that introducing magnetic parameter increases the skin friction coefficient but decreases the heat-transfer rate at the surface.

Kuznetsav and Nield [11] conducted a study to evaluate the effect of nanoparticles on natural convection boundary layer flow past a vertical plate.

They prepared the simplest boundary conditions in which both temperature and nanoparticle fractions were constant along the wall.

Bachok et al. [12] examined the boundary layer flow of nanofluids over a moving surface in a flowing fluid. Ibrahim and Shanker [13] have analyzed the boundary-layer flow and heat transfer due to a stretching sheet. They discussed the effects of unsteadiness parameter, magnetic field and Prandtl number on the flow and heat transfer characteriztics. They indicated that the temperature decreased with an increase in the value of the unsteadiness parameter, magnetic field, and Prandtl number. Ishak et al. [14] numerically examined heat transfer over a stretching surface with variable heat flux in micropolar fluids using Keller-box method. It was found that the local Nusselt number is higher for micropolar fluids when compared to Newtonian fluids.

Again, some of useful researches have been conducted to simulate boundary layer flow of nanofluid under different conditions and geometries [15-18].

Most previous studies on the boundary-layer flow and heat transfer are based on the linear plate stretching velocity ($U_w=CX$), where the global self-similarity solutions are valid. The present analysis provides a deep insight into the boundary layer flow and the heat transfer for the newtonian nanofluids over a stretching sheet with the sheet velocity distribution of the form ($U_w=CX^{\beta}$) and the wall temperature distribution of the form ($T_w=T_\infty+ax^r$); where x denotes the distance from the slit from which the surface emerges and c and a are constants, β and r denote, the sheet velocity exponent and the temperature exponent, respectively.

To the authors' knowledge no attempt has been made yet to analyze the effects of variable sheet velocity distribution and variable wall temperature distribution on the lamina

r boundary layer flow and heat transfer of newtonian nanofluid over a stretching sheet under the combined influence of different nanoparticles and uniform magnetic field. Therefore, this paper can be used as a bridge to fill the knowledge gap. It is an extension of the work of Rana and Bhargava [19] through introducing additional parameter such as temperature parameter in the presence of magnetic field.

In this article we employ an extensively validated, highly efficient, variational finite element code to study this problem.

The governing nonlinear partial differential equations are first transformed into ordinary differential equations and they are then solved numerically using the Keller-box method, an implicit finite-difference scheme.

The aim of the present paper is to investigate the effects of Magnetic field (Mn), Prandtl number (Pr), volume fraction of the nanofluid (Φ), velocity parameter (β) and temperature parameter (r) on the local Nusselt number (Nu_x), skin friction coefficient (Cf_x), dimensionless temperature (θ(η)), dimensionless velocity (f'(η)) and etc. The present study is of immediate interest to all those processes which are highly affected with heat enhancement concept e.g. cooling of metallic sheets or electronic chips etc.

Governing equations

Consider the steady, laminar boundary layer flow and heat transfer of a viscous and incompressible nanofluid over a stretching sheet.

In this two-dimensional model, rectangular Cartesian coordinates (x,y) are used, in which the x- and y-axes are taken as the coordinates parallel to the plate and normal to it, respectively, and the nanofluid occupies the region y≥0. The coordinate system and scheme of the problem is shown in Figure 1.

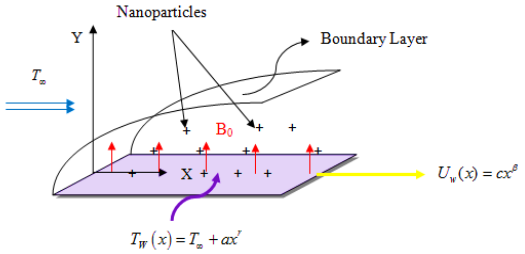

Fig. 1. Physical model and coordinate system

It is assumed that the sheet moves with a velocity distribution of the form ($U_w=cx^\beta$) and is subject to a prescribed surface temperature, i.e.($T_w=T_\infty+ax^r$). The flow is subjected to a transverse magnetic field of strength B_0 which is assumed to be applied in the positive y-direction, normal to the surface.

The fluid is a water based nanofluid containing different types of nanoparticles such as Copper Cu, Silver Ag, Alumina Al_2O_3, Copper oxide CuO and Titanate TiO_2. The thermo physical properties of the nanofluid are given in Table 1. (see Mahdy[20]).

Table1

Thermo-physical properties of water and nanoparticles.

Base fluid and nanoparticles	ρ (Kgm^{-3})	C_p ($Jkg^{-1}K^{-1}$)	K ($Wm^{-1}K^{-1}$)
Pure Water(H_2O)	997.1	4179	0.6130
Copper(Cu)	8933	385.0	401.00
CopperOxide(Cuo)	3620	531.8	76.500
Silver(Ag)	10500	235.0	429.00
alumina(Al_2O_3)	3970	765.0	40.000
TitaniumOxide (TiO_2)	4250	686.2	8.9538

It is also assumed that:

1. The base fluid and the nanoparticles are in thermal equilibrium and no slip occurs between them.
2. The thermo-physical properties of the nanofluids are constant.
3. Viscous dissipation and radiative heat transfer are negligible.
4. The influence of surface tension on the flow is negligible.

With these assumptions, the basic equations governing the velocity and temperature fields of the nanofluid over a stretching sheet can be written as follows

$$\frac{\partial u}{\partial x}+\frac{\partial v}{\partial y}=0 \tag{1}$$

$$u\frac{\partial u}{\partial x}+v\frac{\partial u}{\partial y}=\frac{\mu_{nf}}{\rho_{nf}}\frac{\partial^2 u}{\partial y^2}-\frac{\sigma B_0^2}{\rho_{nf}}u \tag{2}$$

$$u\frac{\partial T}{\partial x}+v\frac{\partial T}{\partial y}=\frac{k_{nf}}{\left(\rho C_p\right)_{nf}}\frac{\partial^2 T}{\partial y^2} \tag{3}$$

Considering the following boundary conditions

$$\begin{aligned} &u(x,0)=U_w=cx^\beta,\ v(x,0)=0,\\ &T(x,0)=T_w=T_\infty+ax^r\\ &u\to 0,\quad T\to T_\infty \quad at \quad y\to\infty \end{aligned} \tag{4}$$

where, u and *v* are the velocity components along the axes x and y, respectively, σ is the electrical conductivity, B_0 is the uniform magnetic field, ρ_{nf} is the effective density of the nanofluid, μ_{nf} is the effective dynamic viscosity of the nanofluid. K_{nf} is the effective thermal conductivity of the nanofluid, T is the temperature of the nanofluid and $(\rho c_p)_{nf}$ is the heat capacity of the nanofluid. Now, we introduce the following dimensionless function ψ(x,y), θ(η) and the similarity variable η as Prasad et al. [21], Xu and Liao[22].

$$\theta(\eta)=\frac{T-T_\infty}{T_w-T_\infty},\quad \eta=\frac{y}{x}\mathrm{Re}_x^{(\frac{1}{2})},\qquad \Psi(x,y)=U_w x(\mathrm{Re}_x)^{\frac{-1}{2}}.f(\eta) \tag{5}$$

Where ψ(x,y) is the stream function which defines in usual way by $u=\frac{\partial\psi(x,y)}{\partial y}$, $v=-\frac{\partial\psi(x,y)}{\partial x}$ and Re_x is the local Reynolds number which defines as $Re_x=U_w.x/\ \nu_f$. The transformed momentum and energy equations together with the boundary conditions given by equations (2-4) can be written as

$$f'''+\phi_1.\left[\left(\frac{\beta+1}{2}\right)ff''-\beta f'^2-Mnf'\right]=0 \tag{6}$$

$$\theta''+\phi_2\ \mathrm{Pr}_f\ .\left[\left(\frac{\beta+1}{2}\right)f\theta'-rf'\theta\right]=0 \tag{7}$$

Where pr_f is the Prandtl number which defines as $pr_f=(\mu C_p)_f/k_f$, β and r denote respectively the sheet velocity exponent and the temperature exponent, $Mn=\sigma B_0^2/\rho_{rf}$ is the magnetic parameter and the constants Φ_1, Φ_2 that depend on the volume fractions are respectively given by

$$\phi_1=\frac{\mu_f}{\mu_{nf}}\left[(1-\phi)+\phi\left(\frac{\rho_p}{\rho_f}\right)\right] \tag{8-a}$$

$$\phi_2=\left(\frac{k_f}{k_{nf}}\right).\left[(1-\phi)+\phi\left(\frac{(\rho C_p)_p}{(\rho C_p)_f}\right)\right] \tag{8-b}$$

The transformed boundary conditions are

$$f'(0)=1,\quad f(0)=0,\quad \theta(0)=1,\quad f'(\infty)=0,\quad \theta(\infty)=0 \tag{9}$$

The parameters of engineering interest in heat transfer problems are the skin friction coefficient C_f and the Nusselt number Nu_x. These parameters characterize the surface drag and heat transfer rates. The shear stress at the stretching surface τ_w is defined as

$$\tau_w=-\mu_{nf}\left.\frac{\partial u}{\partial y}\right|_{y=0} \tag{10}$$

The local Nusselt number and the skin friction coefficient at the stretching surface are given by

$$Nu_x=-\left(\frac{k_{nf}}{k_f}\right)\mathrm{Re}_x^{(\frac{1}{2})}\theta'(0) \tag{11}$$

$$Cf_x=\frac{2\tau_w}{\rho U_w^{\ 2}}=-2\frac{\mu_{nf}}{\mu_f}\mathrm{Re}_x^{(\frac{-1}{2})}\ f''(0) \tag{12}$$

Thermophysical properties of nanofluid

Different models of viscosity and thermal conductivity have been used by researchers to model the effective viscosity and thermal conductivity of nanofluid as a function of volume fraction.

Now, for nanofluids, let us introducing the expression for ρ_{nf} and $(\rho c_p)_{nf}$ of the nanofluid as [20]:

$$\rho_{nf}=(1-\phi)\rho_f+\phi\rho_p \tag{13}$$

$$(\rho c_p)_{nf}=(1-\phi)(\rho c_p)_f+\phi(\rho c_p)_p \tag{14}$$

The effective viscosity of the Al_2O_3–water nanofluid is approximated by the correlation provided by Masoumi et al. [23]:

$$\frac{\mu_{nf}}{\mu_f}=1+\left(\frac{\rho_p V_b d_p^2}{72N\delta}\right) \tag{15}$$

Where $\delta=[(\pi)/(6\Phi)]^{1/3}\times d_p$ is center to center distance of nanoparticles, $V_b=\frac{1}{d_p}\sqrt{\frac{18k_bT}{\pi\rho_p d_p}}$ is Brownian velocity of nanoparticles and $N=(c_1\Phi+c_2)d_p+(c_3\Phi+c_4)$ is a parameter for adapting the results with experimental data when in $c_1=-1.133\times10^{-6}$, $c2=-2.771\times10^{-6}$, $c_3=9.0\times10^{-8}$ and $c_4=-3.93\times10^{-7}$.

The thermal conductivity of the Al_2O_3–water nanofluid is calculated from Chon et al. [24], which is expressed in the following form:

$$\frac{k_{nf}}{k_f}=1+64.7\phi^{0.746}\left(\frac{d_f}{d_p}\right)^{0.369}\times\left(\frac{k_p}{k_f}\right)^{0.747}Pr_f^{0.9955}\ Re_p^{1.23221} \tag{16}$$

Where, $Re_p=\rho_f k_b T/3\pi\mu^2 l_f$ is the Reynolds number of nanoparticles, k_b is the Boltzmann constant, $(=1.3807\times10^{-23})$ and l_f is the free average distance of water molecules that according to Chon and et al.'s suggestion is taken as 17 nm. Some research also approved the accuracy of this model [25]. The effective viscosity of the Cuo –water nanofluid is determined by Nguyen et al. [26](the diameter of nanoparticles is taken 29nm).

$$\frac{\mu_{nf}}{\mu_f}=1.475-0.319\phi+0.051\phi^2+0.009\phi^3 \tag{17}$$

The khanafer and vafai [27] formula is used for the thermal conductivity of the Cuo –water nanofluid, which is expressed as

$$\frac{k_{nf}}{k_f} = 1 + 1.0112\phi + 2.43275\phi\left(\frac{47}{d_p}\right) - 0.0248\phi\left(\frac{k_p}{0.613}\right) \tag{18}$$

The viscosity of the TitaniumOxide (TiO_2)–water nanofluid can be determined from the following equation [27]:

$$\frac{\mu_{nf}}{\mu_f} = 1 + 3.544\phi + 169.46\phi^2 \tag{19}$$

On the other hand, effective thermal conductivity can be calculated from the well-known formula Bruggeman[28]:

$$\frac{k_{nf}}{k_f} = \frac{1}{4}\left[(3\phi - 1)\frac{k_p}{k_f} + \{3(1-\phi) - 1\} + \sqrt{\Lambda}\right]$$
$$\Lambda = \left[(3\phi - 1)\frac{k_p}{k_f} + \{3(1-\phi) - 1\}\right]^2 + 8\frac{k_p}{k_f} \tag{20}$$

The effective thermal conductivity of the Ag-water and Cu-water nanofluid are approximated by the Maxwell–Garnett model [29] as

$$k_{nf} = k_f\left[\frac{(k_p + 2k_f) - 2\phi(k_f - k_p)}{(k_p + 2k_f) + \phi(k_f - k_p)}\right] \tag{21}$$

The effective viscosity of the Ag-water and Cu-water nanofluid as given by Brinkman [30] is

$$\mu_{nf} = \mu_f / (1-\phi)^{2.5} \tag{22}$$

Although the use of the above thermal conductivity model is restricted to nanoparticles of spherical shape it is found to be very appropriate for studying heat transfer enhancement using nanofluids (see [31-33]).

Φ is volume fraction of the nanofluid, μ_f is the dynamic viscosity of the base fluid, respectively, ρ_f and ρ_p are the densities of the base fluid and nanoparticle, k_f and k_p are the thermal conductivities of the base fluid and nanoparticle, respectively.

The properties of the nanofluids shown in the above subjects are calculated from water and nanoparticle properties at average bulk temperature.

Numerical procedure

The numerical solution for the above coupled ordinary differential equations 6 and 7 for different values of velocity parameter, magnetic parameter, temperature parameter, volume fraction of the nanofluid and Prandtl number is obtained using implicit finite difference scheme called Keller-box method. The Keller-box method has the following four main steps:

1. Reduce the equation or system of equations to a first order system.
2. Write the difference equations using central differences.
3. Linearize the resulting algebraic equations (if they are nonlinear) by Newton's method.
4. Write them in matrix–vector form and use the block-tridiagonal-elimination technique to solve the linear system.

Reduction of Nth order differential equations to N first order equation

As the variations of flow across the boundary layer is more important than along the boundary layer; (because the variations of temperature and velocity across the boundary layer are very much).

Therefore, a typical grid structure along the horizontal coordinate is shown in Figure 2.

Now, we introduce new dependent variables f,u,v,θ and p such that

$$f' = u, \quad u' = v, \quad \theta' = p \tag{23}$$

so that equations 6 and 7 can be written as

$$v' + \phi_1.\left[\left(\frac{\beta+1}{2}\right)fv - \beta u^2 - Mnu\right] = 0 \tag{24-a}$$

$$p' + \phi_2\,\mathrm{Pr}_f.\left[\left(\frac{\beta+1}{2}\right)fp - ru\theta\right] = 0 \tag{24-b}$$

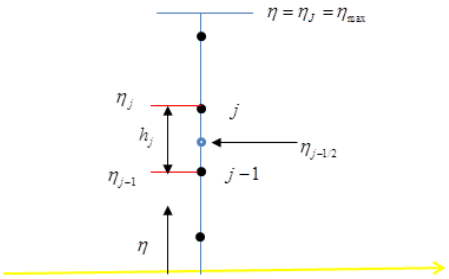

Fig. 2. Typical grid structure for difference approximations

The finite difference discretization

We now consider the geometry of problem as shown in Figure 2 and the net points are defined as follows:

$$\eta_0 = 0, \quad \eta_j = \eta_{j-1} + h_j, \quad j = 1, 2, ..., J, \quad \eta_J = \eta_\infty \tag{25}$$

Where, h_j is the $\Delta\eta$ spacing. We employ the notation $()_j^\eta$ for points and quantities midway between net points and for any net function:

$$\eta_{j-\frac{1}{2}} = \frac{1}{2}\left(\eta_j + \eta_{j-1}\right), \quad ( )^n_{j-\frac{1}{2}} = \frac{1}{2}\left[( )^n_j + ( )^n_{j-1} \right] \tag{26}$$

The superscripts n and n-1 refer, respectively, to the current and previous iteration levels. We start by writing the finite difference form of equation 23 for the midpoint $(\eta_{j-\frac{1}{2}})$ of the j-1, j using centered-difference derivatives.
This process is called centering about $(\eta_{j-\frac{1}{2}})$. We get

$$f' = u_{j-\frac{1}{2}} \Rightarrow \frac{f_j - f_{j-1}}{h_j} = \frac{1}{2}\left(u_j + u_{j-1}\right) \tag{27-a}$$

$$u' = v_{j-\frac{1}{2}} \Rightarrow \frac{u_{j-1} - u_{j-1}}{h_j} = \frac{1}{2}\left(v_j + v_{j-1}\right) \tag{27-b}$$

$$\theta' = p_{j-\frac{1}{2}} = \frac{\theta_j - \theta_{j-1}}{h_j} = \frac{p_j + p_{j-1}}{2} \tag{27-c}$$

Equations (24-a) and (24-b) are also approximated by centering about $\left(\eta_{j-\frac{1}{2}}\right)$ we obtain

$$\begin{aligned} v' &= \frac{v_j - v_{j-1}}{h_j} = \\ &\phi_1.[\beta(u^2) - ((\beta+1)/2) fv + Mn(u)]_{j-\frac{1}{2}} = \\ &\phi_1.\left[\begin{array}{l} \frac{[\beta(u^2) - ((\beta+1)/2) fv + Mn(u)]_j}{2} + \\ \frac{[\beta(u^2) - ((\beta+1)/2) fv + Mn(u)]_{j-1}}{2} \end{array}\right] \end{aligned} \tag{28-a}$$

$$\begin{aligned} p' &= \frac{p_j - p_{j-1}}{h_j} = \\ &-\phi_2.Pr_f\left[\begin{array}{l} \frac{\beta+1}{2}\frac{(fp)_j + (fp)_{j-1}}{2} - \\ r\frac{(u\theta)_j + (u\theta)_{j-1}}{2} \end{array}\right] \end{aligned} \tag{28-b}$$

linearization of non-linear algebraic equation by Newton's method

We assume that $f_j^n, u_j^n, V_j^n, \theta_j^n, p_j^n$ to be known for $0 \le j \le J$. To linearize the nonlinear system of equations (27-a, b and c) using Newton's method, we introduce the following iterate:

$$f_j^{n+1} = f_j^n + \delta f_j^n + \circ\left(\delta^2\right) \tag{29-a}$$

$$u_j^{n+1} = u_j^n + \delta u_j^n + \circ\left(\delta^2\right) \tag{29-b}$$

$$v_j^{n+1} = v_j^n + \delta v_j^n + \circ\left(\delta^2\right) \tag{29-c}$$

$$\theta_j^{n+1} = \theta_j^n + \delta\theta_j^n + \circ\left(\delta^2\right) \tag{29-d}$$

$$p_j^{n+1} = p_j^n + \delta p_j^n + \circ\left(\delta^2\right) \tag{29-e}$$

Substituting these expressions into equations (27-a, b and c) and then dropping the quadratic and higher-order terms in $\delta f_j^n, \delta u_j^n, \delta V_j^n, \delta\theta_j^n, \delta p_j^n$, procedure yields the following linear tridiagonal system:

$$\delta f_j^n - \delta f_{j-1}^n - \frac{h_j}{2}(\delta u_j^n + \delta u_{j-1}^n) = r_j^n \tag{30-a}$$

$$\delta u_j^n - \delta u_{j-1}^n - \frac{h_j}{2}(\delta v_j^n + \delta v_{j-1}^n) = t_j^n \tag{30-b}$$

$$\delta\theta_j^n - \delta\theta_{j-1}^n - \frac{h_j}{2}(\delta p_j^n + \delta p_{j-1}^n) = q_j^n \tag{30-c}$$

$$\left[\begin{array}{l} \frac{h_j}{2}\phi_1.((\beta+1)/2)(v_{j-1}^n \delta f_{j-1}^n + v_j^n \delta f_j^n) - \\ h_j \beta.\phi_1.(u_{j-1}^n \delta u_{j-1}^n + u_j^n \delta u_j^n) + \\ (1 + \frac{h_j}{2}.\phi_1.((\beta+1)/2) f_j^n)\delta v_j^n + \\ (-1 + \frac{h_j}{2}.\phi_1.((\beta+1)/2) f_{j-1}^n)\delta v_{j-1}^n - \\ \frac{h_j}{2}.\phi_1.Mn(\delta u_j^n + \delta u_{j-1}^n) \end{array}\right] = s_j^n \tag{30-d}$$

$$\left[\begin{array}{l} (1 + \frac{h_j}{2}\left(Pr_f.\phi_2.(\beta+1)/2\right) f_j^n)\delta p_j^n + \\ (-1 + \frac{h_j}{2}\left(Pr_f.\phi_2.(\beta+1)/2\right) f_{j-1}^n)\delta p_{j-1}^n + \\ \frac{h_j}{2}\left(Pr_f.\phi_2.(\beta+1)/2\right).(p_{j-1}^n \delta f_{j-1}^n + \\ p_j^n \delta f_j^n) - \frac{h_j}{2}\left(Pr_f.\phi_2.r\right).(\theta_{j-1}^n \delta u_{j-1}^n + \\ \theta_j^n \delta u_j^n) - \frac{h_j}{2}\left(Pr_f.\phi_2.r\right)(u_{j-1}^n \delta\theta_{j-1}^n + \\ u_j^n \delta\theta_j^n) \end{array}\right] = k_j^n \tag{30-e}$$

in which

$$r_j^n = f_{j-1}^n - f_j^n + \frac{h_j}{2}(u_j^n + u_{j-1}^n) \tag{31-a}$$

$$t_j^n = u_{j-1}^n - u_j^n + \frac{h_j}{2}(v_j^n + v_{j-1}^n) \tag{31-b}$$

$$q_j^n = \theta_{j-1}^n - \theta_j^n + \frac{h_j}{2}(p_j^n + p_{j-1}^n) \tag{31-c}$$

$$s_j^n = (v_{j-1}^n - v_j^n) + \phi_1 \cdot \begin{bmatrix} \frac{h_j}{2}[\beta(u_j^2) + \beta(u_{j-1}^2)] + \\ \frac{h_j}{2}[-((\beta+1)/2).v_{j-1}^n f_{j-1}^n - \\ ((\beta+1)/2).v_j^n f_j^n) + Mn(u_j^n + u_{j-1}^n)] \end{bmatrix} \tag{31-d}$$

$$k_j^n = p_{j-1}^n - p_j^n - \phi_2 \cdot \begin{bmatrix} \frac{h_j}{2} \cdot \left(Pr_f \frac{\beta+1)}{2} \right) \cdot (p_j^n f_j^n + p_{j-1}^n f_{j-1}^n) + \\ \frac{h_j}{2} \mathrm{Pr}_f \; r.(\theta_j^n u_j^n + \theta_{j-1}^n u_{j-1}^n) \end{bmatrix} \tag{31-e}$$

To complete the system of equations 30(a-c), we recall the boundary condition which can be satisfied exactly with no iteration. Therefore to maintain these values in all the iterate, we can take

$$\delta f_0 = 0,\ \delta u_0 = 0,\ \delta\theta_0 = 0,\ \delta u_J = 0,\ \delta\theta_J = 0 \tag{32}$$

The block tridiagonal elimination of linear algebraic equations

The linearized difference system of equation 30(a-c) can be solved by block-elimination method as given by Cebeci and Cousteix [34], since the system has a block tridiagonal structure. Most of the time, the block-tridiagonal structure consists of variables or constant but here it consists of block matrices. In a vector-matrix form, the tridiagonal matrix can be written as:

$$A\delta = R \tag{33}$$

The elements of the matrices are defined as follows: where

$$A = \begin{bmatrix} [A_1] & [C_1] & & & & \\ [B_2] & [A_2] & [C_2] & & & \\ & \ddots & \ddots & \ddots & & \\ & & [B_j] & [A_j] & [C_j] & \\ & & & \ddots & \ddots & \ddots \\ & & & & [B_{J-1}] & [A_{J-1}] & [C_{J-1}] \\ & & & & & [B_J] & [A_J] & [C_J] \end{bmatrix}, \quad \delta = \begin{bmatrix} [\delta_1] \\ [\delta_2] \\ \vdots \\ [\delta_j] \\ \vdots \\ [\delta_{J-1}] \\ [\delta_J] \end{bmatrix}, \quad R = \begin{bmatrix} [R_1] \\ [R_2] \\ \vdots \\ [R_j] \\ \vdots \\ [R_{J-1}] \\ [R_J] \end{bmatrix} \tag{34}$$

The elements of the matrices are obtained easily from equations 30 and 31.

To solve equation 33, we assume that matrix A is non-singular and can be factored into

$$A = LU \tag{35}$$

Where

$$L = \begin{bmatrix} [\alpha_1] & & & & \\ [B_2] & [\alpha_2] & & & \\ & \ddots & \ddots & & \\ & & [B_{J-1}] & [\alpha_{J-1}] & \\ & & & [B_J] & [\alpha_J] \end{bmatrix} \tag{36-a}$$

$$U = \begin{bmatrix} [I] & [\Gamma_1] & & & \\ & [I] & [\Gamma_2] & & \\ & & \ddots & \ddots & \\ & & & [I] & [\Gamma_{J-1}] \\ & & & & [I] \end{bmatrix} \tag{36-b}$$

Where [I] is the identity matrix of order 5 and $[\alpha_i]$, and $[\Gamma_i]$ are 5×5 matrices which elements are determined by the following equations:

$$[\alpha_1] = [A_1] \tag{37-a}$$

$$[A_1][\Gamma_1] = [C_1] \tag{37-b}$$

$$[\alpha_j] = [A_j] - [B_j][\Gamma_{j-1}], \quad j = 2, 3, ..., J \tag{37-c}$$

$$[\alpha_j][\Gamma_j] = [C_j], \quad j = 2, 3, ..., J-1 \tag{37-d}$$

Equation 35 can now be substituted into equation 33 and we get

$$[L][U][\delta] = [R] \tag{38}$$

If we define

$$[U][\delta] = [W] \tag{39}$$

then equation 31 becomes

$$[L][W] = [R] \tag{40}$$

Where $W = [[W_1] \; [W_2] \; \ldots \; [W_{J-1}] \; [W_J]]^T$ and the $[W_j]$ are 5×1 column matrices. The elements W can be solved from equation 40.

$$[\alpha_1][W_1] = [R_1] \tag{41}$$

$$\left[\alpha_j\right]\left[W_j\right]=\left[R_j\right]-\left[B_j\right]\left[W_{j-1}\right],\quad 2\le j\le J \tag{42}$$

The step in which $[\Gamma_j]$, $[\alpha_j]$ and $[W_j]$ are calculated is usually refers to as the forward sweep. Once the elements of W are found, equation 39 gives the solution for δ in the so called backward sweep, in which the elements are obtained by the following relations:

$$\left[\delta_J\right]=\left[W_J\right] \tag{43}$$

$$\left[\delta_j\right]=\left[W_j\right]-\left[\Gamma_j\right]\left[\delta_{j+1}\right],\quad 1\le j\le J-1 \tag{44}$$

Once the elements of δ are found, equation 31 can be used to find the (n+1)th iteration. These calculations are repeated until convergence criterion is satisfied and Calculations are stopped when

$$\left|\delta_0^n\right|<\varepsilon \tag{45}$$

Where ε is a small prescribed value. In this study, $\varepsilon=10^{-5}$ is used.

RESULTS AND DISCUSSION

The non-linear differential equation 6 and 7 with appropriate boundary conditions given in equation 9 are difficult to get a closed form solution. These equations are solved numerically, by the most efficient implicit finite difference method. Therefore, FORTRAN code is used to solve the forthcoming continuity, momentum and energy conservation equations for incompressible Newtonian nanofluids. In this study the boundary condition for η at ∞ are replaced by a sufficiently large value of η where the velocity and temperature approaches to zero. Several nodes (10, 40, 80 and 160) were examined to perform a grid independency test. Figure 3 shows the non-dimensional temperatures distributions of Al_2O_3–water nanofluid computed by different grid sizes, which leads to choose the optimum and accurate grid size of $\Delta\eta=0.01$ in η for other numerical computations performed in this study.

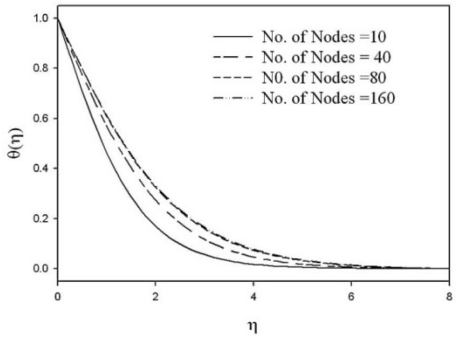

Fig. 3. The non-dimensional temperatures distributions for mesh indepency investigation at $Pr_f=\beta=1$, Mn=0.5 and $r=\Phi=0$

The local Nusselt number of the fluid in terms of $-\theta'(0)$ for pure water when Mn=r=0 and $\beta=1$ is compared with those reported by Ibrahim and Shanker[13], Mahdy[20], Ishak et al. [35], Ali [36], Grubka and Bobba [37].

We observe from Table 2, that the present results are found to be in excellent agreement with the earlier published results.

Table 2
Comparison results of $-\theta'(0)$ for various values of Prandtl numbers (Prf) when Mn=r=0 and $\beta=1$.

Previous Works	Pr_f=0.01	Pr_f=0.72	Pr_f=1.0
Ibrahim and Shanker[13]	----------	0.8095	1.0001
Mahdy[20]	0.0199	0.8086	----------
Ishak [35]	0.0197	0.8086	1.0
Ali [36]	----------	0.8058	----------
Grubka and Bobba [37]	0.0197	0.8086	----------
Present Work	0.0197	0.8086	1.0

In order to validate the employed computer program, a comparison of velocity distributions between the present work and Ibrahim and Shanker [13] for values of Mn=β=1, r=Φ=0 and $Pr_f=0.72$ is presented in Figure 4.

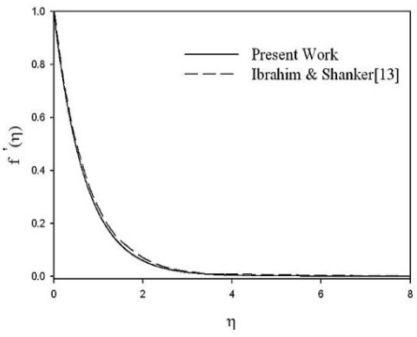

Fig. 4. Comparison of velocity distributions between the present work and Ibrahim and Shanker [13] for values of $Pr_f=0.72$, Mn=β=1 and r=Φ=0

The sample of velocity f′(η) and temperature θ(η) profiles presented in Figures (5–17) show that the boundary conditions (9) are satisfied, which support the presented numerical results.

Figures 5 and 6 exhibit the velocity and temperature distributions of Al_2O_3–water nanofluid for different velocity parameter (the sheet velocity exponent), respectively when Mn=r=0.5 and Φ=0.05.

It is observed that increasing velocity parameter results in a decrease in the thermal boundary layer thickness, associated with an increase in the wall temperature gradient, and hence produces an increase in the surface heat transfer rate. However, a different trend is observed for the velocity profiles as presented in Fig. 5, where smaller boundary layer thickness does not imply larger velocity gradient at the surface (see Figure14 and16).

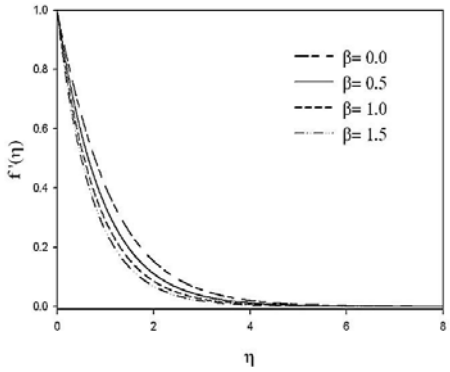

Fig. 5. Velocity distributions for various values of velocity parameter when Mn=r=0.5 and Φ=0.05

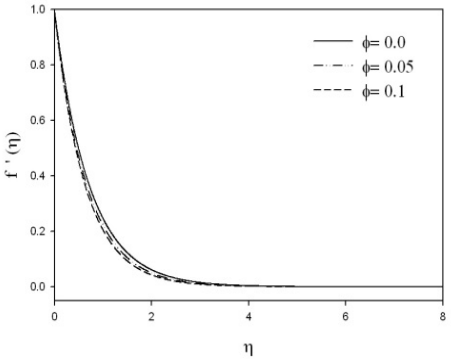

Fig. 7. Velocity distributions for various values of volume fraction of nanoparticles (Φ)when β=Mn=0.5and r=0.2

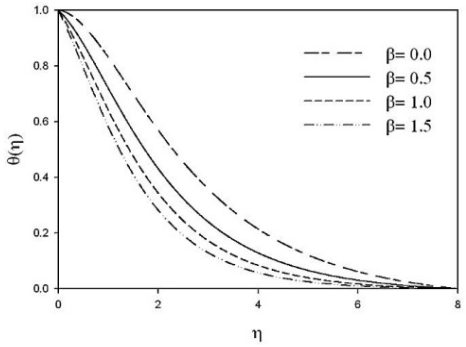

Fig. 6. Temperature distributions for various values of velocity parameter when Mn=r=0.5 and Φ=0.05

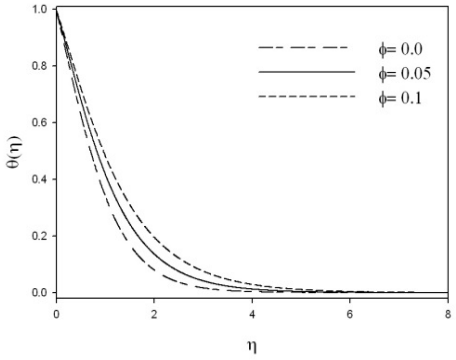

Fig. 8. Temperature distributions for various values of volume fraction of nanoparticles (Φ)when β=Mn=0.5and r=0.2

The effects of the solid volume fraction Φ containing Al_2O_3–water nanoparticles on the velocity and temperature distributions are shown in figures 7 and 8 respectively when Mn=β=0.5 and r=0.2. The figure reveals that, the thermal boundary layer increases continuously with the volume fraction of the nanoparticles.

In addition, adding nanoparticle to the pure water leads to decrease velocity profile while increase temperature profiles.

This agrees with the physical behavior that any increase in volume fraction, increases the inertia forces because the effective density of the nanofluid will be increased and accordingly increases the temperature gradient. Besides, the nanoparticles increase the thermal conductivity ratio term as it can be seen from equation 16.

Therefore, both the temperature gradient term and thermal conductivity ratio term increase by increasing the volume fraction of nanoparticles. Accordingly, it can be seen that with increasing volume fraction temperature distributions will be increased, because the heat transfer properties are improved. Furthermore, we recall from equation 15 that increasing values of ϕ contribute to the enhancement of nanofluid viscosity.

As the viscosity increases it offers considerable drag to fluid flow thereby slowing down its motion.

Figures 9 and 10 show the velocity and temperature distributions of Al_2O_3–water nanofluid for different magnetic parameter Mn, respectively when β=r=0.5 and Φ=0.05.

It is observed that flow velocity profile decreases with an increase in the magnetic characteristic. This causes retarding effect on the flow field which leads to the prominent reduction in velocity profile due to Lorentz force effect.

Therefore, the Lorentz force which opposes the motion of nanofluid increases with the increase in Mn. It is also noticed from the Figure 10 that the temperature profile θ increases with increasing values of magnetic parameter in the boundary layer.

This is due to additional work expended in dragging the nanofluid in the boundary layer against the action of the Lorentz force and energy is dissipated as thermal energy which heats the nanofluid.

This induces a rise in temperature. Furthermore, the graph shows that the thermal boundary-layer thickness slightly increases with an increase in magnetic parameter Mn. The effects of different nanoparticles on the temperature distributions θ and velocity profiles f′(η) are shown, when Mn=1, β=r=0.5 and Φ=0.1, in Figures 11 and 12.

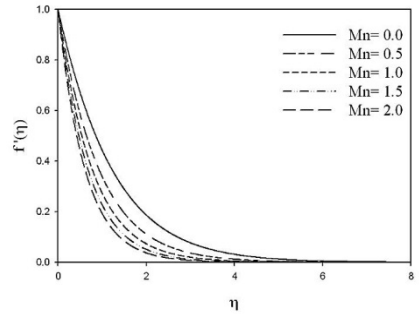

Fig. 9. Velocity distributions for various values of magnetic parameter (Mn) when β=r=0.5 and Φ=0.05

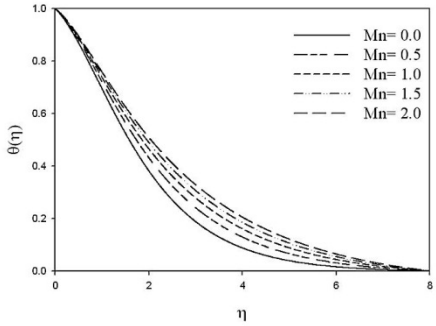

Fig.10. Temperature distributions for various values of magnetic parameter (Mn) when β=r=0.5 and Φ=0.05

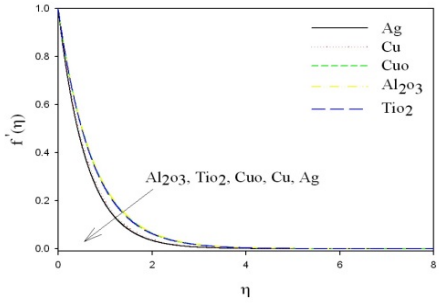

Fig. 11. Velocity distributions for different types of nanoparticles when Mn=1, β=r=0.5 and Φ=0.1

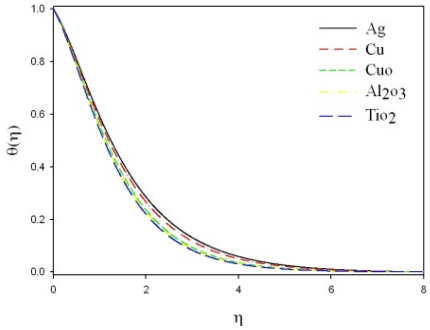

Fig. 12. Temperature distributions for different types of nanoparticles when Mn=1, β=r=0.5 and Φ=0.1

It can be observed that the velocity and temperature distributions for different nanoparticles decrease gradually far away from the surface of the stretching sheet. Moreover, a slight increasing in the velocity and temperature distributions can be detected by adding different nanoparticles to the base fluid. Therefore, both Figures 11 and 12 exhibit that the addition of different types of nanoparticles in water improve the velocity profiles and temperature distributions. Moreover, it can be observed that the velocity profiles and the temperature distributions are not strongly affected by additional various nanoparticles with low solid volume fraction concentrations. In addition, it can be noticed in Figure 12 that the temperature profiles of Ag–water nanofluid are the higher one and normally greater than the pure water.

These Figures show that on using different kinds of nanofluids the velocity and temperature change, which means that the nanofluids will be important in the cooling and heating processes. In Figure 13, the effect of temperature parameter (r) on temperature distributions is investigated for pure water, when Pr_f=1 and Mn=β=0.5. As shown in Figure 13, the non-dimensional temperature profiles increase as the temperature distribution parameter r decreases in the boundary layer.

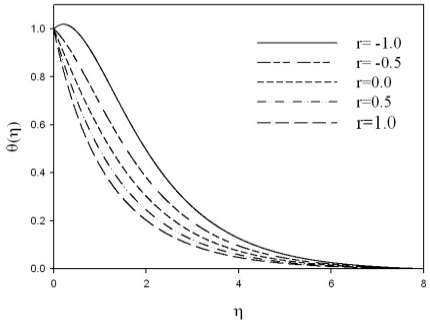

Fig. 13. Temperature distributions for some values of temperature parameter (r) when Pr_f=1 and Mn=β=0.5

Figure 14, shows the skin friction coefficient of Al_2O_3–water nanofluid for different volume fraction of Al_2O_3 nanoparticle and velocity parameter, when Mn=r=0.5.

Figure 15 shows the skin friction coefficient of Al_2O_3–water nanofluid for different volume fraction of Al_2O_3 nanoparticle and velocity parameter, when β=r=0.5. It is seen from both Figures 14 and 15, the skin friction coefficient decreases as volume fraction of Al_2O_3 nanoparticle increases in the boundary layer. This is because any increase in volume fraction, increases the wall shear stress because the effective viscosity of the nanofluid will be increased as it can be seen from equation 15 and accordingly increases the skin friction coefficient.

Figures 14 and 15 also reveal that, the skin friction coefficient of Al_2O_3–water nanofluid decreases continuously with an increase in the magnetic and velocity parameters.

It is now a well established fact that the magnetic field presents a damping effect on the velocity field by creating drag force that opposes the fluid motion, causing

the velocity to decease.

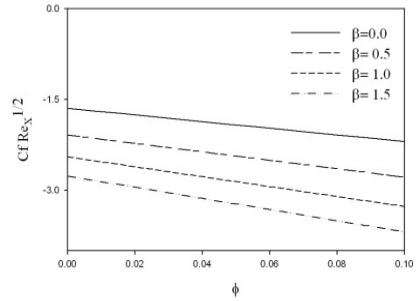

Fig. 14. The skin friction coefficient of Al_2O_3–water nanofluid for different volume fraction and velocity parameter when Mn=r=0.5

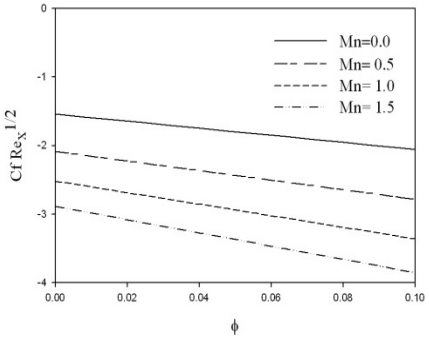

Fig. 15. The skin friction coefficient of Al_2O_3–water nanofluid for different volume fraction and magnetic parameter when $\beta = r = 0.5$

The effects of different volume fraction of Al_2O_3 nanoparticle, magnetic and velocity parameters on the local Nusselt number are shown in Figures 16 and 17. (Figure 16 and Figurre 17 is plotted, respectively when Mn=r=0.5 and β=r=0.5). It is found that by increasing volume fraction of nanofluid, the local Nusselt number raises which consequently increases heat transfer in the boundary layer. Figure 16 also reveals that, the local Nusselt number of Al_2O_3–water nanofluid increases continuously with an increase in the velocity parameter. As shown in Figure 17 increasing the magnetic parameter leads to decrease the local Nusselt number in the boundary layer.

The effects of the solid volume fraction containing Al_2O_3–water nanoparticles and magnetic parameter on temperature distributions are investigated in Table 3, respectively when β=r=0.5 and η=2. It can be seen in this Table, the dimensionless temperature increases slightly due to increase in volume fraction of Al_2O_3 nanoparticles and magnetic parameter.

It is also found that the role of magnetic parameter on dimensionless temperature becomes more significant in the low value. For instance, at Φ=0.05 when magnetic parameter is 0.0, 0.5, 1.0, 1.5 and 2, dimensionless temperature will gain the value of 0.3816, 0.4317, 0.4653, 0.4898 and 0.5088, respectively. The analysis reveals that, the combined influence of nanoparticles and uniform magnetic field over a stretching sheet at β=r=0.5, Φ=0.1 and Mn=0.5 makes a heat transfer enhancement about 31% while at same condition this value is about 35%, 37.5% and 39% respectively for Mn=1.0, Mn=1.5 and Mn=2.0. This example and other presented data in Figure 10, clearly present that the magnetohydrodynamic flow (MHD) becomes more effective in lower magnetic parameter.

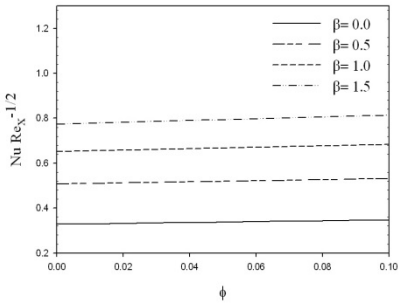

Fig. 16. The local Nusselt number of Al_2O_3–water nanofluid for different volume fraction and velocity parameter when Mn=r=0.5

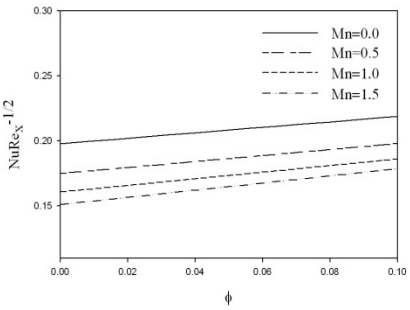

Fig. 17. The local Nusselt number of Al_2O_3–water nanofluid for different volume fraction and magnetic parameter when β=r=0.5

Table 3
Comparison results of dimensionless temperature for various values of ϕ and Mn when $\eta = 2$ and β=r=0.5.

	$\theta(\eta)$		
	$\phi = 0.0$	$\phi = 0.05$	$\phi = 0.1$
Mn=0.0	0.3293	0.3816	0.4285
Mn=0.5	0.3812	0.4317	0.4751
Mn = 1.0	0.4174	0.4653	0.5053
Mn = 1.5	0.4446	0.4898	0.5270
Mn = 2.0	0.4659	0.5088	0.5435

Conclusions

In this paper, the boundary layer flow and heat transfer of MHD Newtonian nanofluids over a stretching sheet with the sheet velocity distribution of the form $U_w=cx^\beta$ and the wall temperature distribution of the form $T_w=T_\infty+ax^r$ are studied.

The boundary layer equations governing the flow are reduced to a set of non-linear ordinary differential equations using a similarity transformation. The numerical results are presented for nanofluid with a wide range of Magnetic parameter (Mn), volume fraction of different

nanoparticles (Ag, Cu, CuO, Al_2O_3 and Tio_2), velocity parameter (β) and temperature parameter (r). Briefly the above discussion can be summarized as follows:

1) Comparison with known results for steady state flow is presented and it found to be in excellent agreement.

2) For all considered cases, when the volume fraction of the nanoparticles is kept constant, the rate of heat transfer increases by increase of the Magnetic parameter.

3) It is also illustrated that the role of magnetic parameter on dimensionless temperature becomes more effective in lower value.

4) The thermal boundary layer thickness decreases with an increase in velocity and temperature parameters.

5) The momentum boundary layer thickness decreases with an increase in the volume fraction of nanoparticles, velocity and magnetic parameters.

6) The velocity profiles decrease with the increase in the volume fraction of nanoparticles and velocity parameter.

7) Increasing the magnetic parameter leads to decrease the local Nusselt number and the skin friction coefficient in the boundary layer.

8) It can also be seen that the temperature profile of Ag–water nanofluid is higher than other studied nanofluids.

9) The thermal boundary layer increases and momentum boundary layer decreases with the use of water based nanofluids as compared to pure water.

10) The non-dimensional temperature profiles increase with the increase in the volume fraction of nanoparticles and magnetic parameter.

REFERENCES

[1] U.S. Choi: Enhancing thermal conductivity of fluids with nanoparticle Developments and Applications of Non-Newtonian Flows 231 (1995) 99-105.

[2] S. Choi, Z. Zhang, W. Yu, F. Lockwood, E. Grulke: Anomalously thermal conductivity enhancement in nanotube suspensions, Journal of Applied Physics Letters 79 (2001) 2252–2254.

[3] S. Z. Heris, M. N. Esfahany, S. Gh. Etemad : Experimental Investigation of Convective Heat Transfer of Al_2O_3/Water Nanofluid in Circular Tube, International Journal of Heat and Fluid Flow 28 (2006) 203–210.

[4] M. Hojjat, S. Etemad, R. Bagheri: Laminar heat transfer of non-Newtonian nanofluids in a circular tube, Korean Journal of Chemical Engineering 27 (2010) 1391–1396.

[5] B.C. Pak, Y. Cho: Hydrodynamic and heat transfer study of dispersed fluids with submicron metallic oxide particles, Experimental Heat Transfer 11 (1998) 151-170.

[6] Y. Xuan, Q. Li: Investigation on convective heat transfer and flow features of nanofluids, Journal of Heat Transfer 125 (2003) 151-155.

[7] A. Ahuja: Augmentation of heat transport in laminar flow of polystyrene suspensions, Journal of Applied Physics 46 (1975) 3408-3425.

[8] J. Buongiorno: Convective transport in nanofluids, Journal of Heat Transfer 128 (2006) 240-250.

[9] MA Fadzilah, R Nazar, M. Arifin, I. Pop: MHD boundary-layer flow and heat transfer over a stretching sheet with induced magnetic field. Journal of Heat Mass Transfer 47 (2011) 155–162.

[10] A. Ishak, R. Naza, I. Pop: MHD boundary-layer flow due to a moving extensible surface, Journal of Engineering Mathematics 62 (2008) 23–33.

[11] A.V. Kuznetsov, D.A Nield: Natural convective boundary-layer flow of a nanofluid past a vertical plate, International Journal of Thermal Sciences 49 (2010) 243-247.

[12] N. Bachok, A.Ishak, I.Pop: Boundary-layer flow of nanofluids over a moving surface in a flowing fluid, International Journal of Thermal Sciences 49 (2010) 1663-1668.

[13] W.Ibrahim, B. Shanker: Unsteady MHD boundary-layer flow and heat transfer due to stretching sheet in the presence of heat source or sink, International Journal of Computers & Fluids 70 (2012) 21-28.

[14] A. Ishak, R. Naza, I. Pop: Heat transfer over a stretching surface with variable heat flux in microplar fluids. Physics Letters A 5 (2008) 559–61.

[15] A. Noghrehabadi, R. Pourrajab, M. Ghalambaz: Effect of partial slip boundary condition on the flow and heat transfer of nanofluids past stretching sheet prescribed constant wall temperature, International Journal of Thermal Sciences 54 (2012) 253-261

[16] M. Narayana, P. Sibanda: Laminar flow of a nanoliquid film over an unsteady stretching sheet, International Journal of Heat and Mass Transfer 55 (2012) 7552-7560.

[17] A. Aziz, W.A. Khan: Natural convective boundary layer flow of a nanofluid past a convectively heated vertical plate, International Journal of Thermal Sciences 52 (2012) 83-90.

[18] L. Zheng, C. Zhang, X. Zhang, J. Zhang: Flow and radiation heat transfer of a nanofluid over a stretching sheet with velocity slip and temperature jump in porous medium, Journal of the Franklin Institute 350 (2013) 990–1007.

[19] P. Rana, R. Bhargava: Flow and heat transfer of a nanofluid over a nonlinearly stretching sheet: A numerical study, Communications in Nonlinear Science and Numerical Simulation 17 (2012) 212–226.

[20] A. Mahdy: Unsteady mixed convection boundary layer flow and heat transfer of nanofluids due to stretching sheet, Nuclear Engineering and Design 249 (2012) 248– 255.

[21] K.V. Prasad, P.S. Pal Dulal, Datti: MHD power-law fluid flow and heat transfer over a non-isothermal stretching sheet, Communications in Nonlinear Science and Numerical Simulation 14 (2009) 2178

–2189.

[22] H. Xu, S. Liao: Laminar flow and heat transfer in the boundary-layer of non-Newtonian fluids over a stretching flat sheet, Computers and Mathematics with Applications 57 (2009) 1425_1431.

[23] N. Masoumi, N. Sohrabi, A.A. Behzadmehr: New model for calculating the effective viscosity of nanofluids, Journal of Physics D: Applied Physics 42 (2009) 055501–055506.

[24] C.H. Chon, K.D. Kihm, S.P. Lee, S.U. Choi: Empirical correlation finding the role of temperature and particle size for nanofluid (Al_2O_3) thermal conductivity enhancement, Journal of Applied Physics Letters 87 (2005) 153107–153110.

[25] H.A. Mintsa, G. Roy, C.T. Nguyen, D. Doucet: temperature dependent thermal conductivity data for water-based nanofluids, International Journal of Thermal Sciences 48 (2009) 363–371.

[26] C.T Nguyen., F. s Desgrange, G. Roy, T. Galanis, S. Boucher, H.A.n Mintsa: Temperature and particle-size dependent viscosity data for waterbased nanofluids–hysteresis phenomenon, International Journal of Heat Fluid Flow 28 (2009) 1492–1506.

[27] Kh. Khanafer, K. Vafai: A critical synthesis of thermophysical characteristics of nanofluids, International Journal of Heat Mass Transfer 54 (2011) 4410–4428.

[28] D.A.G. Bruggeman: Berechnung verschiedener-physikalischer konstanten von heterogenen substanzen, I. Dielektrizitatskonstanten und leitfahigkeiten der mischkorper aus isotropen substanzen, Annals of Physics 24 (1935) 636– 679.

[29] J.C. Maxwell Garnett : Colours in metal glasses and in metallic films, Philos. Trans. R. Soc. Lond. A 203 (1904). 385–420.

[30] H.C. Brinkman: The viscosity of concentrated suspensions and solutions. Journal of Chemical Physics 20 (1952) 571–581.

[31] S.E.B. Maiga, S.J. Palm, C.T.Nguyen, G. Roy, N. Galanis: Heat transfer enhancement by using nanofluids in forced convection flow, International Journal of Heat and Fluid Flow 26 (2005) 530–546.

[32] E. Abu-Nada: Application of nanofluids for heat transfer enhancement of separated flows encountered in a backward facing step, International Journal of Heat Fluid Flow 29 (2008) 242–249.

[33] A. Akbarinia, A. Behzadmehr: Numerical study of laminar mixed convection of a nanofluid in horizontal curved tubes, Journal of Applied Thermal Engineering 27 (2007) 1327–1337.

[34] T. Cebeci, J. Cousteix: Modeling and Computation of Boundary-Layer Flows, Second Edition, Horizons Publishing Inc., Long Beach, California-Springer-Verlag, (2005).

[35] A. Ishak, R. Nazar, I. Pop: Boundary layer flow and heat transfer over an unsteady stretching vertical surface Meccanica 44 (2009) 369–375.

[36] M.E.Ali: Heat transfer characteristics of a continuous stretching surface, Journal of Heat Mass Transfer 29 (1904) 227–234.

[37] L.J. Grubka, K.M. Bobba: Heat transfer characteristi -cs of a continuous, stretching surface with variable temperature, ASME Journal of Heat Transfer 107 (1985) 248–250.